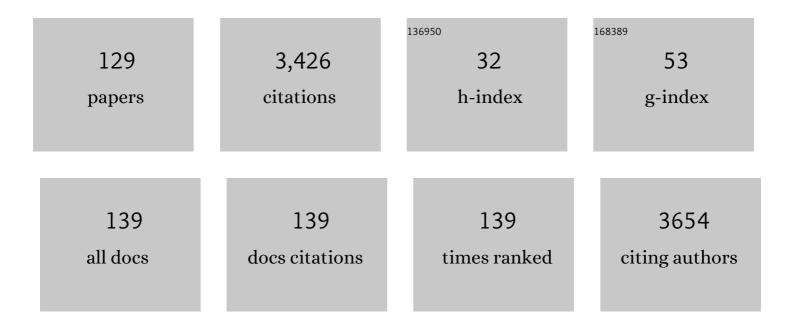
List of Publications by Year in descending order

Source: https://exaly.com/author-pdf/9054763/publications.pdf Version: 2024-02-01



ΔΟΛΤΛ Δ ΕΥΝΕΡ

#	Article	IF	CITATIONS
1	Pharmacokinetic Modeling of the Second-Wave Phenomenon in Nanobubble-Based Contrast-Enhanced Ultrasound. IEEE Transactions on Biomedical Engineering, 2023, 70, 42-54.	4.2	1
2	Iridium(III) Complex-Loaded Perfluoropropane Nanobubbles for Enhanced Sonodynamic Therapy. Bioconjugate Chemistry, 2022, 33, 1057-1068.	3.6	7
3	Effects of shell-integrated Sudan Black dye on the acoustic activity and ultrasound imaging properties of lipid-shelled nanoscale ultrasound contrast agents. Journal of Biomedical Optics, 2022, 27, .	2.6	0
4	Intracellular vesicle entrapment of nanobubble ultrasound contrast agents targeted to PSMA promotes prolonged enhancement and stability <i>in vivo</i> and <i>in vitro</i> . Nanotheranostics, 2022, 6, 270-285.	5.2	10
5	Development of a novel castrationâ€resistant orthotopic prostate cancer model in New Zealand White rabbit. Prostate, 2022, 82, 695-705.	2.3	5
6	Extrusion: A New Method for Rapid Formulation of High‥ield, Monodisperse Nanobubbles. Small, 2022, 18, e2200810.	10.0	9
7	Sonotheranostics and Sonogenetics Special Issue. Bioconjugate Chemistry, 2022, 33, 991-992.	3.6	1
8	Formulation of a Thermosensitive Imaging Hydrogel for Topical Application and Rapid Visualization of Tumor Margins in the Surgical Cavity. Cancers, 2022, 14, 3459.	3.7	2
9	Ultrasound-Based Molecular Imaging of Tumors with PTPmu Biomarker-Targeted Nanobubble Contrast Agents. International Journal of Molecular Sciences, 2021, 22, 1983.	4.1	14
10	Molecular imaging of orthotopic prostate cancer with nanobubble ultrasound contrast agents targeted to PSMA. Scientific Reports, 2021, 11, 4726.	3.3	18
11	Toward Precisely Controllable Acoustic Response of Shell-Stabilized Nanobubbles: High Yield and Narrow Dispersity. ACS Nano, 2021, 15, 4901-4915.	14.6	43
12	Microfluidic Generation of Monodisperse Nanobubbles by Selective Gas Dissolution. Small, 2021, 17, e2100345.	10.0	20
13	High-Frequency Array-Based Nanobubble Nonlinear Imaging in a Phantom and <i>In Vivo</i> . IEEE Transactions on Ultrasonics, Ferroelectrics, and Frequency Control, 2021, 68, 2059-2074.	3.0	3
14	Ultrasound Triggered Drug Release from Affinity-Based β-Cyclodextrin Polymers for Infection Control. Annals of Biomedical Engineering, 2021, 49, 2513-2521.	2.5	2
15	Bursting microbubbles: How nanobubble contrast agents can enable the future of medical ultrasound molecular imaging and image-guided therapy. Current Opinion in Colloid and Interface Science, 2021, 54, 101463.	7.4	45
16	Biodegradable cascade nanocatalysts enable tumor-microenvironment remodeling for controllable CO release and targeted/synergistic cancer nanotherapy. Biomaterials, 2021, 276, 121001.	11.4	35
17	The dance of the nanobubbles: detecting acoustic backscatter from sub-micron bubbles using ultra-high frequency acoustic microscopy. Nanoscale, 2020, 12, 21420-21428.	5.6	8
18	Photoacoustic imaging biomarkers for monitoring biophysical changes during nanobubble-mediated radiation treatment. Photoacoustics, 2020, 20, 100201.	7.8	16

#	Article	IF	CITATIONS
19	Concurrent visual and acoustic tracking of passive and active delivery of nanobubbles to tumors. Theranostics, 2020, 10, 11690-11706.	10.0	29
20	Improving Treatment Efficacy of In Situ Forming Implants via Concurrent Delivery of Chemotherapeutic and Chemosensitizer. Scientific Reports, 2020, 10, 6587.	3.3	6
21	Increasing Doxorubicin Loading in Lipid-Shelled Perfluoropropane Nanobubbles via a Simple Deprotonation Strategy. Frontiers in Pharmacology, 2020, 11, 644.	3.5	18
22	Contrast-enhanced ultrasound with sub-micron sized contrast agents detects insulitis in mouse models of type1 diabetes. Nature Communications, 2020, 11, 2238.	12.8	37
23	In situ forming implants exposed to ultrasound enhance therapeutic efficacy in subcutaneous murine tumors. Journal of Controlled Release, 2020, 324, 146-155.	9.9	9
24	Delayed response to proton beam treatment of hepatocellular carcinoma. BJR case Reports, 2020, 6, 20180125.	0.2	1
25	Theoretical and Experimental Gas Volume Quantification of Micro- and Nanobubble Ultrasound Contrast Agents. Pharmaceutics, 2020, 12, 208.	4.5	27
26	Real time ultrasound molecular imaging of prostate cancer with PSMA-targeted nanobubbles. Nanomedicine: Nanotechnology, Biology, and Medicine, 2020, 28, 102213.	3.3	41
27	Pickering Bubbles as Dual-Modality Ultrasound and Photoacoustic Contrast Agents. ACS Applied Materials & Interfaces, 2020, 12, 22308-22317.	8.0	19
28	Contrast enhanced ultrasound imaging by nature-inspired ultrastable echogenic nanobubbles. Nanoscale, 2019, 11, 15647-15658.	5.6	86
29	Enhancing Tumor Drug Distribution With Ultrasound-Triggered Nanobubbles. Journal of Pharmaceutical Sciences, 2019, 108, 3091-3098.	3.3	52
30	Time-intensity-curve Analysis and Tumor Extravasation of Nanobubble Ultrasound Contrast Agents. Ultrasound in Medicine and Biology, 2019, 45, 2502-2514.	1.5	60
31	Sink or float? Characterization of shell-stabilized bulk nanobubbles using a resonant mass measurement technique. Nanoscale, 2019, 11, 851-855.	5.6	62
32	PMMA-Fe <sub>3</sub> O <sub>4</sub> for internal mechanical support and magnetic thermal ablation of bone tumors. Theranostics, 2019, 9, 4192-4207.	10.0	62
33	Influence of Nanobubble Concentration on Blood–Brain Barrier Opening Using Focused Ultrasound Under Real-Time Acoustic Feedback Control. Ultrasound in Medicine and Biology, 2019, 45, 2174-2187.	1.5	24
34	An artificially engineered "tumor bio-magnet―for collecting blood-circulating nanoparticles and magnetic hyperthermia. Biomaterials Science, 2019, 7, 1815-1824.	5.4	10
35	Tunable Polymer Embolic Implant for Vascular Occlusion. ACS Biomaterials Science and Engineering, 2019, 5, 1849-1856.	5.2	0
36	Effect of Bubble Concentration on the in Vitro and in Vivo Performance of Highly Stable Lipid Shell-Stabilized Micro- and Nanoscale Ultrasound Contrast Agents. Langmuir, 2019, 35, 10192-10202.	3.5	48

#	Article	IF	CITATIONS
37	The Effect of Freeze/Thawing on the Physical Properties and Acoustic Performance of Perfluoropropane Nanobubble Suspensions. , 2019, , .		2
38	Radiation-enhanced nanobubble therapy: Monitoring treatment effects using photoacoustic imaging. , 2019, , .		0
39	Quantification of PSMA expression in prostate cancer by pharmacokinetic modeling of targeted ultrasound nanobubbles. , 2019, , .		1
40	In vitro Preparation and Characterization of Magnetic Nanobubbles. , 2019, , .		1
41	Inhibition of the histone demethylase, KDM5B, directly induces re-expression of tumor suppressor protein HEXIM1 in cancer cells. Breast Cancer Research, 2019, 21, 138.	5.0	20
42	Individual nanobubbles detection using acoustic based flow cytometry. , 2019, , .		0
43	Role of Surface Tension in Gas Nanobubble Stability Under Ultrasound. ACS Applied Materials & Interfaces, 2018, 10, 9949-9956.	8.0	52
44	Porphyrin-Loaded Pluronic Nanobubbles: A New US-Activated Agent for Future Theranostic Applications. Bioconjugate Chemistry, 2018, 29, 234-240.	3.6	36
45	Polymer Nanosheet Containing Star‣ike Copolymers: A Novel Scalable Controlled Release System. Small, 2018, 14, e1800115.	10.0	5
46	Dual-Targeted Microbubbles Specific to Integrin αVβ3 and Vascular Endothelial Growth Factor Receptor 2 for Ultrasonography Evaluation of Tumor Angiogenesis. Ultrasound in Medicine and Biology, 2018, 44, 1460-1467.	1.5	21
47	Nanobubble Extravasation in Prostate Tumors Imaged with Ultrasound: Role of Active versus Passive Targeting. , 2018, , .		11
48	Ultrasound-Enhanced Distribution and Treatment Efficacy of Dox-Loaded Intratumoral In Situ Forming Implants in Murine HCT-15 Tumors. , 2018, , .		2
49	The Effect of Lipid Solubilization on the Performance of Doxorubicin-Loaded Nanobubbles. , 2018, , .		4
50	Nanobubble Facilitated Optoporation and Photoacoustic Imaging of BT-474 Breast Cancer Cells. , 2018, , .		1
51	Acoustic Actuation of Integrinâ€Bound Microbubbles for Mechanical Phenotyping during Differentiation and Morphogenesis of Human Embryonic Stem Cells. Small, 2018, 14, e1803137.	10.0	15
52	Ultrasound Contrast Agents and Delivery Systems in Cancer Detection and Therapy. Advances in Cancer Research, 2018, 139, 57-84.	5.0	67
53	Characterization of different bubble formulations for blood-brain barrier opening using a focused ultrasound system with acoustic feedback control. Scientific Reports, 2018, 8, 7986.	3.3	71
54	Abstract 260: Apigenin nanoparticle suppresses sphere formation in CD133+/ALDH1highprostate cancer stam cells through downregulation of stem cell markers 2018		1

stem cells through downregulation of stem cell markers. , 2018, , .

#	Article	IF	CITATIONS
55	Predicting in vivo behavior of injectable, in situ-forming drug-delivery systems. Therapeutic Delivery, 2017, 8, 479-483.	2.2	6
56	Cryo-EM Visualization of Lipid and Polymer-Stabilized Perfluorocarbon Gas Nanobubbles - A Step Towards Nanobubble Mediated Drug Delivery. Scientific Reports, 2017, 7, 13517.	3.3	52
57	Increasing Distribution of Drugs Released from In Situ Forming PLGA Implants Using Therapeutic Ultrasound. Annals of Biomedical Engineering, 2017, 45, 2879-2887.	2.5	11
58	Ultrasound molecular imaging of ovarian cancer with CA-125 targeted nanobubble contrast agents. Nanomedicine: Nanotechnology, Biology, and Medicine, 2017, 13, 2159-2168.	3.3	102
59	Improving performance of nanoscale ultrasound contrast agents using N,N-diethylacrylamide stabilization. Nanomedicine: Nanotechnology, Biology, and Medicine, 2017, 13, 59-67.	3.3	79
60	Theoretical and experimental investigation of the nonlinear dynamics of nanobubbles excited at clinically relevant ultrasound frequencies and pressures: The role of lipid shell buckling. , 2017, , .		2
61	Enhancing fluorescein release from in-situ forming PLGA implants using therapeutic ultrasound. , 2017, , .		Ο
62	Ultrasound signal from sub-micron lipid-coated bubbles. , 2017, , .		1
63	Effect of the surfactant pluronic on the stability of lipid-stabilized perfluorocarbon nanobubbles. , 2017, , .		2
64	Enhancing fluorescein distribution from in situ forming PLGA implants using therapeutic ultrasound. , 2017, , .		1
65	Ultrasound characterization of slow precipitating implants for vascular occlusion. , 2017, , .		0
66	Using ultrasound and photoacoustics to monitor in situ forming implant structure and drug release. , 2017, , .		1
67	Notice of Removal: Nanobubble contrast agents enhance ultrasound imaging of prostate tumors in mice. , 2017, , .		0
68	Ultrasound signal from sub-micron lipid-coated bubbles. , 2017, , .		4
69	Effect of the surfactant pluronic on the stability of lipid-stabilized perfluorocarbon nanobubbles. , 2017, , .		0
70	Theoretical and experimental investigation of the nonlinear dynamics of nanobubbles excited at clinically relevant ultrasound frequencies and pressures: The role oflipid shell buckling. , 2017, , .		1
71	Notice of Removal: On the fate of mesh-stabilized lipid nanobubbles after destruction with ultrasound. , 2017, , .		3
72	Using ultrasound and photoacoustics to monitor in situ forming implant structure and drug release. , 2017, , .		0

#	Article	IF	CITATIONS
73	Ultrasound characterization of slow precipitating implants for vascular occlusion. , 2017, , .		Ο
74	Efficiency of combined blocking of aerobic and glycolytic metabolism pathways in treatment of N1-S1 hepatocellular carcinoma in a rat model. Journal of Cancer Research and Therapeutics, 2017, 13, 533-537.	0.9	5
75	Ultrasound-guided intratumoral delivery of doxorubicin from <i>in situ</i> forming implants in a hepatocellular carcinoma model. Therapeutic Delivery, 2016, 7, 201-212.	2.2	13
76	Nondestructive Characterization of Biodegradable Polymer Erosion in Vivo Using Ultrasound Elastography Imaging. ACS Biomaterials Science and Engineering, 2016, 2, 1005-1012.	5.2	8
77	Macroporous acrylamide phantoms improve prediction of in vivo performance of in situ forming implants. Journal of Controlled Release, 2016, 243, 225-231.	9.9	27
78	Induction of HEXIM1 activities by HMBA derivative 4a1: Functional consequences and mechanism. Cancer Letters, 2016, 379, 60-69.	7.2	9
79	Image-Guided Development of Biomaterials: Enabling Technologies Shaping and Expediting the Future of Materials in Medicine. Annals of Biomedical Engineering, 2016, 44, 619-620.	2.5	1
80	Development of a High-Throughput Ultrasound Technique for the Analysis of Tissue Engineering Constructs. Annals of Biomedical Engineering, 2016, 44, 793-802.	2.5	6
81	Validation of Ultrasound Elastography Imaging for Nondestructive Characterization of Stiffer Biomaterials. Annals of Biomedical Engineering, 2016, 44, 1515-1523.	2.5	7
82	Post radiofrequency ablation assessment of colorectal cancer liver metastases—does post ablation biopsy really matter?. Translational Cancer Research, 2016, 5, S411-S414.	1.0	0
83	Effect of the Subcutaneous Environment on Phase-Sensitive In Situ-Forming Implant Drug Release, Degradation, and Microstructure. Journal of Pharmaceutical Sciences, 2015, 104, 4322-4328.	3.3	29
84	The Effect of Additives on the Behavior of Phase Sensitive In Situ Forming Implants. Journal of Pharmaceutical Sciences, 2015, 104, 3471-3480.	3.3	24
85	Ultrasound imaging beyond the vasculature with new generation contrast agents. Wiley Interdisciplinary Reviews: Nanomedicine and Nanobiotechnology, 2015, 7, 593-608.	6.1	79
86	Biomedical Imaging in Implantable Drug Delivery Systems. Current Drug Targets, 2015, 16, 672-682.	2.1	33
87	Real-time Monitoring of Radiofrequency Ablation and Postablation Assessment: Accuracy of Contrast-enhanced US in Experimental Rat Liver Model. Radiology, 2014, 270, 107-116.	7.3	47
88	Nanobubble Ultrasound Contrast Agents for Enhanced Delivery of Thermal Sensitizer to Tumors Undergoing Radiofrequency Ablation. Pharmaceutical Research, 2014, 31, 1407-1417.	3.5	52
89	Acoustic Characterization and Pharmacokinetic Analyses of New Nanobubble Ultrasound Contrast Agents. Ultrasound in Medicine and Biology, 2013, 39, 2137-2146.	1.5	117
90	MultimodalIn Vivolmaging Exposes the Voyage of Nanoparticles in Tumor Microcirculation. ACS Nano, 2013, 7, 3118-3129.	14.6	59

#	Article	IF	CITATIONS
91	Inhibition of metastasis by HEXIM1 through effects on cell invasion and angiogenesis. Oncogene, 2013, 32, 3829-3839.	5.9	29
92	Research Spotlight: Applications of ultrasound for image-guided drug delivery in cancer chemotherapy. Therapeutic Delivery, 2013, 4, 785-789.	2.2	2
93	Preclinical evaluation of radiosensitizing activity of Pluronic block copolymers. International Journal of Radiation Biology, 2013, 89, 801-812.	1.8	7
94	Differentiation of Benign Periablational Enhancement from Residual Tumor Following Radio-Frequency Ablation Using Contrast-Enhanced Ultrasonography in a Rat Subcutaneous Colon Cancer Model. Ultrasound in Medicine and Biology, 2012, 38, 443-453.	1.5	13
95	Radiofrequency Ablation: Effect of Tumor- and Organ-specific Pharmacologic Modulation of Arterial and Portal Venous Blood Flow on Coagulation Diameter in an N1-S1 Tumor Model. Journal of Vascular and Interventional Radiology, 2012, 23, 826-832.	0.5	3
96	Noninvasive Characterization of the Effect of Varying PLGA Molecular Weight Blends on <i>In Situ</i> Forming Implant Behavior Using Ultrasound Imaging. Theranostics, 2012, 2, 1064-1077.	10.0	50
97	Electrospinning and Imaging. Advanced Engineering Materials, 2012, 14, B266.	3.5	17
98	Effect of cargo properties on in situ forming implant behavior determined by noninvasive ultrasound imaging. Drug Delivery and Translational Research, 2012, 2, 45-55.	5.8	30
99	Structural parameters governing activity of Pluronic triblock copolymers in hyperthermia cancer therapy. International Journal of Hyperthermia, 2011, 27, 663-671.	2.5	23
100	Role of Pluronic block copolymers in modulation of heat shock protein 70 expression. International Journal of Hyperthermia, 2011, 27, 672-681.	2.5	11
101	Noninvasive characterization of in situ forming implants using diagnostic ultrasound. Journal of Controlled Release, 2010, 143, 183-190.	9.9	65
102	Effect of injection site on in situ implant formation and drug release in vivo. Journal of Controlled Release, 2010, 147, 350-358.	9.9	92
103	Characterization of formulation parameters affecting low molecular weight drug release from <i>in situ</i> forming drug delivery systems. Journal of Biomedical Materials Research - Part A, 2010, 94A, 476-484.	4.0	43
104	Advances in image-guided intratumoral drug delivery techniques. Therapeutic Delivery, 2010, 1, 307-322.	2.2	23
105	Formulation and Characterization of Echogenic Lipidâ^'Pluronic Nanobubbles. Molecular Pharmaceutics, 2010, 7, 49-59.	4.6	117
106	Image-Guided Therapeutics. Molecular Pharmaceutics, 2010, 7, 1-2.	4.6	6
107	Time and Dose Dependence of Pluronic Bioactivity in Hyperthermia-Induced Tumor Cell Death. Experimental Biology and Medicine, 2009, 234, 95-104.	2.4	18
108	Vasomodulation of Tumor Blood Flow: Effect on Perfusion and Thermal Ablation Size. Annals of Biomedical Engineering, 2009, 37, 552-564.	2.5	13

#	Article	IF	CITATIONS
109	0079: Direct Measurement of Blood Flow Velocity in Small Diameter Vessels Using Contrast-Enhanced Ultrasound. Ultrasound in Medicine and Biology, 2009, 35, S16.	1.5	4
110	Dynamic Evolutionary Changes in Blood Flow Measured by MDCT in a Hepatic VX2 Tumor Implant over an Extended 28-day Growth Period: Time-Density Curve Analysis. Academic Radiology, 2009, 16, 1483-1492.	2.5	18
111	Radiofrequency Ablation. Academic Radiology, 2009, 16, 321-331.	2.5	11
112	Model simulation and experimental validation of intratumoral chemotherapy using multiple polymer implants. Medical and Biological Engineering and Computing, 2008, 46, 1039-1049.	2.8	22
113	Drug-eluting polymer implants in cancer therapy. Expert Opinion on Drug Delivery, 2008, 5, 775-788.	5.0	52
114	Combination of Sensitizing Pretreatment and Radiofrequency Tumor Ablation: Evaluation in Rat Model. Radiology, 2008, 246, 796-803.	7.3	17
115	Semiquantitative imaging measurement of baseline and vasomodulated normal prostatic blood flow using sildenafil. International Journal of Impotence Research, 2007, 19, 110-113.	1.8	7
116	Combined radiofrequency ablation and doxorubicin-eluting polymer implants for liver cancer treatment. Journal of Biomedical Materials Research - Part A, 2007, 81A, 205-213.	4.0	31
117	Modeling doxorubicin transport to improve intratumoral drug delivery to RF ablated tumors. Journal of Controlled Release, 2007, 124, 11-19.	9.9	51
118	Effect of intratumoral injection of carboplatin combined with pluronic P85 or L61 on experimental colorectal carcinoma in rats. Experimental Biology and Medicine, 2007, 232, 950-7.	2.4	14
119	Injectable Polymer Depot Combined With Radiofrequency Ablation for Treatment of Experimental Carcinoma in Rat. Investigative Radiology, 2006, 41, 890-897.	6.2	25
120	Enhancement of carboplatin toxicity by Pluronic block copolymers. Journal of Controlled Release, 2005, 106, 188-197.	9.9	77
121	Combined Tumor Therapy by Using Radiofrequency Ablation and 5-FU–Laden Polymer Implants: Evaluation in Rats and Rabbits. Radiology, 2005, 237, 911-918.	7.3	29
122	TECHNIQUES IN X-RAY COMPUTED TOMOGRAPHY IN THE EVALUATION OF DRUG RELEASE SYSTEMS AND THEIR APPLICATION. , 2005, , 105-131.		0
123	A feasibility study of high intensity focused ultrasound for liver biopsy hemostasis. Ultrasound in Medicine and Biology, 2004, 30, 1531-1537.	1.5	7
124	Quantitative computed tomography analysis of local chemotherapy in liver tissue after radiofrequency ablation1. Academic Radiology, 2004, 11, 1326-1336.	2.5	7
125	Noninvasive Monitoring of Local Drug Release Using X-ray Ccomputed Tomography: Optimization and In Vitro/In Vivo Validation. Journal of Pharmaceutical Sciences, 2003, 92, 289-296.	3.3	25
126	X-ray computed tomography methods for in vivo evaluation of local drug release systems. IEEE Transactions on Medical Imaging, 2002, 21, 1310-1316.	8.9	14

#	Article	IF	CITATIONS
127	Noninvasive monitoring of local drug release in a rabbit radiofrequency (RF) ablation model using X-ray computed tomography. Journal of Controlled Release, 2002, 83, 415-425.	9.9	15
128	Combined modeling and experimental approach for the development of dual-release polymer millirods. Journal of Controlled Release, 2002, 83, 427-435.	9.9	25
129	Agarose gel stiffness determines rate of DRG neurite extension in 3D cultures. Biomaterials, 2001, 22, 1077-1084.	11.4	470